Postprint of: Szmytkowski J., Głowienka D., Verger M., Gorter H., Dogan I., Verhees W., Najafi M., Veenstra S., Galagan Y., Additive Effect of Bromides and Chlorides on the Performance of Perovskite Solar Cells Fabricated via Sequential Deposition, JOURNAL OF POWER SOURCES, Vol. 513 (2021), 230528 (2021), DOI: 10.1016/j.jpowsour.2021.230528



# Additive Effect of Bromides and Chlorides on the Performance of Perovskite Solar Cells Fabricated via Sequential Deposition

Jędrzej Szmytkowski[a,], Damian Glowienka[a,b], Manon Verger[b], Harrie Gorter[b], Ilker Dogan[b], Wiljan Verhees[b], Mehrdad Najafi[b], Sjoerd Veenstra[b], Yulia Galagan[c]

[a] *Faculty of Applied Physics and Mathematics, Gdańsk University of Technology Narutowicza 11/12, 80-233 Gdańsk, Poland*
[b] *TNO - Solliance, High Tech Campus 21, Eindhoven 5656AE, The Netherlands*
[c] *Department of Materials Science and Engineering, National Taiwan University, Taipei 10617, Taiwan*

**Abstract**

A two–step sequential deposition method has been applied to prepare the solar cells with two types of perovskites $Cs_{0.15}FA_{0.85}Pb(I_{0.95}Cl_{0.05})_3$ and $Cs_{0.15}FA_{0.85}Pb(I_{0.95}Br_{0.05})_3$. In order to obtain the perovskite layers, the different sources of bromine and chlorine atoms were used for synthesis. The performance and time stability of chloride–based photocells are worse in comparison to the bromide–based devices. It can be explained by the effect of an accumulation of Cl atoms at the interfaces between the chloride–based perovskites and the layer of PCBM. Such a process causes an increasing of interface recombination. Also, the bulk density of states and, consequently, the bulk recombination of charge carriers seem to be higher for the perovskite layers obtained with chlorine atoms. The two–step technique applied to create the bromide perovskites less influences the photocells performance as in the case of one–step deposition. We can explain this observation by an existence of nucleation sites in the inorganic layer which improve the growth of a perovskite material.

*Keywords:* Sequential Deposition, Perovskite Solar Cells

*Email addresses:* jedszmyt@pg.gda.pl ; jedrek@mif.pg.gda.pl (Jędrzej Szmytkowski), ygalagan@ntu.edu.tw (Yulia Galagan)

## 1. Introduction

Solar cells based on hybrid lead halide perovskites employed as active materials are very attractive structures for modern photovoltaics. Besides high efficiency which exceeds 20%, the stable perovskite photocells have been recently reported [1, 2, 3, 4, 5, 6]. However, a mechanistic understanding why some perovskite solar cells exhibit a better stability than others is often lacking. Thus, many efforts are currently focused on finding the optimized preparation technique to obtain most efficient and stable PSCs.

In general, we can find two methods to synthesize the organic–inorganic hybrid perovskites. One method is based on the solution processing and the second technique applies the thermal evaporation [7]. Typically, perovskites synthesized via the solution processing are fabricated using a spin–coating (SC). Initially, researchers prepared the perovskite precursor in one solution which was used to deposit the perovskite layer. Later, it has been demonstrated that such perovskites can be prepared via a two–step technique [8]. First, the inorganic component is deposited on the substrate, followed by the organic part coated on the first layer, both via SC. This two–step method of preparation is often called the sequential deposition technique. It has been reported in many works [9, 10, 11, 12, 13, 14, 15, 16, 17, 18, 19, 20] that the sequential deposition became a good tool to obtain dense and uniform perovskite layers, and also efficient PSCs. However, an inadequate mixing of both precursors can lead to incomplete conversion into the perovskite [21].

Apart from different methods of preparation, the used compounds also influence the performance of PSCs. Recently [22], we have investigated an impact of different bromine sources on the dual cation (2C) perovskite $Cs_{0.18}FA_{0.82}Pb(I_{0.94}Br_{0.06})_3$, which consists of formamidinium (FA) and caesium ions. These studies have been realized using one–step deposition method. The conclusion was that the source of bromine atoms influenced the various complexes during the crystallization process. Therefore, different densities of traps were created in the bulk, which affected the final efficiency. Now, the question is if a two–step process is

also associated with the formation of complex species. Thus, we have decided to test the same sources of bromine atoms (CsBr, $PbBr_2$, FABr) for two–step sequential deposition technique. However, this time we compare bromine photocells with the devices fabricated using similar sources of chlorine atoms (CsCl, $PbCl_2$, FACl). The reason of choosing chlorides stems from the observation that the addition of Cl atoms improves the stability against humidity [23].

In this work, we will study two 2C perovkite materials $Cs_{0.15}FA_{0.85}Pb(I_{0.95}Cl_{0.05})_3$ and $Cs_{0.15}FA_{0.85}Pb(I_{0.95}Br_{0.05})_3$ prepared using two–step sequential deposition method. The main goal of this paper is to understand the dominant recombination mechanisms in these PSCs. Especially that the complex formation influences the bulk defect densities which are strongly related to the trap–assisted recombination of charge carriers [24].

## 2. Experimental section

### *2.1. Device fabrication*

The structure of devices can be written as glass/ITO/PTAA/$CsFAPb(I,X)_3$/PCBM/BCP/Cu, where X is to denote Br or Cl. The compounds and solvents used to create solar cells are presented as follows. Lead iodide ($PbI_2$, 99.99 %), lead bromide ($PbBr_2$, 99 %) and bathocuproine (BCP, >98.0 %) were purchased from TCI. Lead chloride ($PbCl_2$, 99 %) and caesium bromide (CsBr, 99.9 %) were bought from Alfa Aesar. Caesium iodide (CsI, 99.999 %), dimethyl sulfoxide anhydrous (DMSO, 99.9 %), dimethylformamide (DMF, 99.8 %), toluene anhydrous (99.8 %), chlorobenzene anhydrous (99.8 %), ethanol anhydrous (99.8 %), and propan–2–ol anhydrous (IPA, 99.5 %) were obtained from Sigma–Aldrich. Formamidinium iodide (FAI, >99.99 %), formamidinium bromide (FABr, >99.99 %) and formamidinium chloride (FACl, >99.5 %) were purchased from GreatCell Solar. Caesium chloride (CsCl, >99 %) was bought from Across. [6,6]–phenyl–C61–butyric acid methyl ester (PCBM, 99 %) was obtained from Solenne, while poly[bis(4–phenyl)(2,4,6–trimethylphenyl)amine]

(PTAA, grade M) was purchased from Solaris Chem. All commercial materials and solvents were used without purification.

The solar cells were fabricated in a nitrogen filled glove–box. The glass/ITO substrates were cleaned with a soap, rinsed with a deionized water, sonicated in a bath of IPA, dried with a $N_2$ gas spray and put in an UV–ozone oven for 30 min. In order to obtain the hole transporting layer (HTL), PTAA from solution (4 mg in 1 ml toluene) was deposited on the ITO using SC method (5000 rpm, 3000 rpm/s, 35 s). This step was followed by an annealing at 100° C for 10 min. Next, the perovskite layers have been prepared by the two–step sequential deposition technique. Six different perovskite compositions were created. The materials to compose the precursors for both layers are presented in Table 1. The compounds used to prepare first layers were dissolved in 1 ml of DMF:DMSO with the ratio 9:1, while the chemicals for second layers were dissolved in 1 ml of IPA. The second layer was dropped from 80 $\mu$l of the precursor solution just 30 seconds after the beginning of SC of the first layer. Both precursor layers were spin–coated using the same SC parameters for all perovskites (3000 rpm, 3000 rpm/s, 90 s). Afterwards, an annealing was performed at 100° C for 10 min. Later, PCBM has been deposited by SC (1500 rpm, 3000 rpm/s, 50 s) in order to create the electron transporting layer (ETL). For this step, the solution was prepared with 20 mg of PCBM in 1 ml of chlorobenzene and filtered before use. At the top, BCP from solution (1 mg in 1 ml ethanol) was dropped using spin–coating (4000 rpm, 3000 rpm/s, 35 s). Finally, the copper (100 nm) was thermally evaporated (at pressure $10^{-6}$ mbar) on top of the device to create the metal contact.

### *2.2. Characterization*

The crystallographic structures of all perovskites have been characterized using X–ray diffractometer (XRD, PanAlytical Empyrean). The scanning electron microscope (SEM, Jeol JSM–6010LA IntouchScope) has been applied to study the morphology of samples. In order to investigate the optical properties, the transmittance (T) and the reflectance (R) were measured with UV–vis

spectrophotometer (Agilent Cary 5000). The photocurrent–voltage (J–V) characteristics (Keithley 2400) of photocells have been recorded in a nitrogen environment. The white light halogen lamp served as a source of light. To obtain AM 1.5 conditions, a silicon cell has been applied as a reference to calibrate the lamp to 1000 W $m^{-2}$. The masks were used to focus the light on the illuminated devices with the active area equal to 0.09 $cm^2$. The intensity of light has been changed (1, 0.83, 0.53, 0.33, 0.1, 0.01 and 0.001 sun) with a set of filters. In order to analyze the hysteresis effect, the J–V curves were measured in two bias directions: forward (from -0.2 V to 1.1 V) and reverse (from 1.1 V to -0.2 V). The scanning rate for the current detection was 0.165 V $s^{-1}$ with a step of 20 mV. The procedure of photoelectrical measurement has been organized as follows. First, all perovskite solar cells were investigated without illumination. Next, the samples were continuously illuminated to obtain J–V characteristics. The maximum power point tracking (MPPT) has been measured for all photocells for two minutes. In addition, a longer MPPT was later realized for selected samples. It should be noted that this type of the MPP recording was compatible with the ISOS–L–1 protocol [25].

## 3. Results and discussion

In this work, the samples obtained from bromide sources CsBr, $PbBr_2$ and FABr are named Cs–Br, Pb–Br and FA–Br, respectively. The devices prepared with chlorides CsCl, $PbCl_2$ and FACl are called Cs–Cl, Pb–Cl and FA–Cl, respectively.

Fig. 1 illustrates the XRD results obtained for all perovskite compounds prepared on the glass substrate. We can see that the photoactive (black) $\alpha$–phase [26, 27, 28] dominates in each layer. The detailed analysis of the peak positions shows that FA–Br and FA–Cl peaks have slightly different positions for the $\alpha$–phase than in other perovskite layers, see Fig. 1 (insets). According to Vegard's law, the shift toward higher angles is due to the introduction of smaller ions. In our case, caesium exchanges formamidinium, and bromide or

chloride ions substitute iodide ions. Here, we observe a slight shift toward higher angles for the perovskites created without FABr or FACl materials. It would mean that the inclusion of smaller ions is worse in the case of using these formamidinium compounds. The XRD analysis reveals also reflections related to non–perovskite phases. The reason is that the perovskite material has not fully converted into a pure $\alpha$–phase during crystallization and, consequently, some secondary–phases have appeared [29]. The $CsPbI_3$ phase has been detected in all samples. However, it is present with a highest amount in FA–Br and FA–Cl perovskite layers. In addition, all samples (except FA–Cl) contain $PbI_2$ with the highest amount detected in FA–Br sample. This phase is mostly observed at 12.8° peak with (001) orientation. However, other $PbI_2$ peaks are also visible for the perovskites with bromine atoms. It could be related to a not full conversion of the $PbI_2$ material or to a faster degradation of the sample. In general, FA–Br and FA–Cl samples seem to crystallize worse than other samples. We should note that the complex formation observed for one–step deposition method [22] is not visible here.

Fig. S1 presents the UV–vis spectra for perovskite films on the glass substrate. The absorption maxima are related to the electron transitions between hybridized 6s(Pb)/5p(I) orbitals and 6p(Pb) orbitals [30]. Although similar shapes of the absorption spectra are observed for all samples, we can see that FA–Br and FA–Cl perovskites differ slightly from other samples. It confirms the existence of an additional non–perovskite phase visible in XRD results. To conclude, the use of FABr and FACl compounds in the second layer during synthesis causes incomplete crystallization and formation of a secondary phase.

Fig. 2 shows the SEM images of all perovskites prepared on the glass substrate. The needles–like structures have been distinctively seen on the FA–Br and FA–Cl surfaces which can originate from the formation of secondary phases during the crystallization process. These results are in line with XRD and UV–vis analysis. Therefore, the conclusion is that both formamidinium compounds FACl and FABr did not fully react and the observed structures are associated with the secondary phases.

Fig. 3 presents a comparison of four photovoltaic parameters (the power conversion efficiency PCE, the short–circuit current $J_{sc}$, the open–circuit voltage $V_{oc}$ and the fill factor FF) obtained for three types of bromide PSCs measured under 1 sun. We observe that Pb–Br devices are less efficient than Cs–Br and FA–Br solar cells. The drop of PCE by about 3% is mostly due to differences in FF and slightly in $V_{oc}$. It seems that different mechanisms of the crystallization process occur in the samples when various sources of bromine atoms are used for synthesis and, thereby, it affects the density of defect states in the bulk. However, in the two–step sequential deposition method, the source of halogens has a less pronounced effect on PCE than for the single step process. Most likely, the first inorganic layer supports the growth of perovskite film by giving it a nucleation site.

Fig. 4 illustrates four photovoltaic parameters (PCE, $J_{sc}$, $V_{oc}$ and FF) for the chloride–based PSCs measured for light intensity of 1 sun. Here, we observe that Cs–Cl samples are the least efficient, while FA–Cl devices give the best performance. It is clearly seen that the fill factor plays a crucial role here. However, the short–circuit current should have a stronger impact on the efficiency due to a higher statistical spread than for bromide samples.

Fig. 5 demonstrates J–V characteristics obtained for bromide and chloride representative PSCs drawn for the reverse scan. Results from a full measurement cycle which includes both the reverse and the forward directions are additionally presented in Fig. S2. We can see that Cs–Br and FA–Br samples are more efficient than Pb–Br device mostly due to a higher $V_{oc}$ and FF (Fig. 5a). It can be interpreted as a consequence of the bulk recombination effects. Fig. 5b shows results obtained for the chlorine based solar cells. Here, the influence of $V_{oc}$ is negligible due to small variations of this parameter. It looks that mostly $J_{sc}$ and FF impact on the performance which seems to be rather an interface dependent effect [31]. Such a behavior can be associated with the accumulation of chlorine species at the interface between the perovskite and PCBM, because Cl compounds can escape from the bulk of perovskite to its surface during the crystallization. Recent studies have confirmed that chlorine atoms do not built

into the perovskite structure due to several reasons [32]. The Cl atoms can be emitted in a gaseous form of organic chlorides during annealing [33, 34]. If the temperature or the time of annealing are insufficient, then chloride compounds accumulate at the surface which causes an increasing of surface recombination. In addition, the accumulation of chlorine anions can occur also at the interfaces [35]. In this process, the precursor with Cl plays an important role. According to Suzuki et al.[36], the addition of FACl leads to changes of the interface between the perovskite and $TiO_2$ layers. It has been also demonstrated that the blend precursor with $PbCl_2$ or PbICl improves the incorporation of chlorines into the perovskite but it needs a very high formation energy [37]. However, we cannot exclude that this effect is due to the association of Cl with Cs or FA which gives a better fitting location in the crystal structure. Apart from the interfaces, grain boundaries also serve as accumulation centers for chlorines [38, 39, 40]. We believe that, in our experiment, chlorine compounds can accumulate or form a secondary phase layer between the perovskite and PCBM films. This process changes the interface defect states and also the energy alignment which can lead to a band–bending effect and, as a consequence, it causes a decreasing of $J_{sc}$ [41, 42, 43, 44, 45]. We should not observe this effect in the bromine devices, because Br atoms do not accumulate at the interface. However, the bromine species can influence the formation of nucleation sites which improve the growth of a perovskite layer. This process should be visible mainly at the substrate side (ITO/HTL/perovskite). Therefore, we expect a formation of the "dead layer" [46] near the contact of this perovskite with PTAA. In addition, the needle–like structures seen for FA–Br photocells in the SEM image (Fig. 2) create a contact at the ETL side (with PCBM). The exact establishment of these interface positions for both bromine and chlorine devices is proven in the following EQE analysis.

Fig. S3 illustrates the EQE results for bromide– and chloride–based PSCs. No differences are visible between Cs–Br and Pb–Br samples (Fig. S3a). However, a slightly different curve has been obtained for FA–Br solar cell in comparison to other bromide photocells. The distinctions are most explicit at both edges

of the EQE spectrum. It seems that the formamidinium source of bromine atoms affects both interfaces slightly more than bulk of the perovskite. The change in the infrared part 650–800 nm could be associated with the needle–like structures on surface. However, a reason of the observed difference in the range 300–500 nm originates rather from the interface recombination process. We can see that the UV–vis spectrum (Fig. S1) is higher than the EQE curve in this region. It means that a penetration depth of light is small. Therefore we conclude that an "optical dead layer" [46] was formed at the illuminated perovskite/PTAA interface. Fig. S3b shows the EQE spectra for the chloride–based PSCs. Here, one can notice a slight difference for FA–Cl sample in comparison to other devices, which is visible only at the infrared part of the spectrum. This behavior can be explained by the accumulation of chlorine atoms at the interface between the perovskite and PCBM layers. However, we should not neglect also the accumulation of the chloride compound (FACl) which did not fully react.

Fig. 6 shows the influence of light intensity on four photovoltaic parameters (PCE, $J_{sc}$, $V_{oc}$ and FF) measured for the bromide–based PSCs. Recently, we have demonstrated that such experimental results, given for a very wide range of the illumination intensity, can be analyzed with the drift–diffusion simulations to identify the dominant recombination mechanisms [22, 31]. However, although such simulations are helpful in the analysis of light–intensity data, we are able to clearly interpret the experimental results without making the simulations. It should be also mentioned that the typical J–V curves obtained for only 1 sun do not clearly indicate which mechanism dominates in PCE losses. The influence of recombination mechanisms on the value of ideality factor ($n_{id}$) was discussed in the literature [47, 48, 49]. It has been demonstrated that a lowering of the ideality factor causes a decreasing of the bulk recombination and an increasing of the interface recombination. Here, we can see that Cs–Br PSC has a rather high $n_{id}$ equal to 1.748 which is smaller than the value observed for Cs–Br samples obtained using one–step deposition method [22]. This suggests that the bulk recombination is still the main process but the interface recombination also contributes. It agrees with the FF losses at a high light intensity [31].

The fill factor exhibits the peak at approximately 75% which means that about 15% of the FF is lost due to bulk defects, if considering the Shockley–Queisser perfect cell [50]. Fig. 6 shows that the FA–Br samples have a slightly lower ideality factor equal to 1.641. The losses from the bulk recombination should be approximately the same as for the Cs–Br samples. Therefore, the decrease of an ideality factor can be explained by a higher interface recombination. However, the FF drop visible at a higher light intensity cannot stem only from the interface recombination effect, especially for such $V_{oc}$ losses. Thus, this drop of FF seems to be series resistance dependent. As it has been seen in SEM images (Fig. 2), the needles–like structures are observed on the surface of the FA–Br samples. It is possible that these needles are not fully removed during a spin–coating of PCBM and, as a consequence, they form the additional contact between the PCBM and a perovskite. Such an interpretation explains both the interface recombination and series resistance losses and it also stays in agreement with the EQE results (Fig. S2). We can see that the Pb–Br samples exhibit a much higher ideality factor equal to 1.871 and a deeper drop of the FF. At the same time, the shape of the FF dependence versus light intensity is the same as for the Cs–Br PSC. This can be explained by the bulk quality of the perovskite layer that is much more defected due to the crystallization process with the use of $PbBr_2$ as the source of bromine atoms.

Fig. 7 shows four photovoltaic parameters (PCE, $J_{sc}$, $V_{oc}$ and FF) versus the light intensity drawn for the chloride–based PSCs. We can see that the ideality factors of all samples synthesized with different chlorine sources are higher in comparison to the bromide–based PSCs. The FF exhibits similar values for all three types of chloride photocells in a wide range of light intensity, which was not observed for the bromide samples. It is visible that the peak of FF is close to 75%. The highest ideality factor has been observed for the FA–Cl PSC. It is the least affected by the interface recombination which would decrease that value. Also, the losses of FF at 1 sun are the lowest for this sample. We can clearly see that the differences observed for the FFs and ideality factors should be strongly related. This means that the value of the ideality factor decreases for higher

losses of the FF. To conclude, we observe the accumulation of the respective salt at the interfaces which causes that chlorines do not built perfectly into the perovskite structure. This effect influences the interface recombination and, as a consequence, it impacts the FF and ideality factor in this way that both decrease for a higher density of defect states at the interfaces. The short–circuit current $J_{sc}$ changes between Cs–Cl, Pb–Cl and FA–Cl samples for higher light intensities. The explanation of the $J_{sc}$ losses is based on the role of energy alignment in chloride–based perovskite. It deals with a band–bending effect which blocks a charge carrier extraction and leads to decreasing of $J_{sc}$ [41, 42, 43, 44, 45].

The time evolution of a maximum power point (MPP) measured in the best performing PSCs for a short period (300 s) is presented in Fig. 8a. We can see a totally different behavior between all perovskites. The observed differences in the MPP between representative samples are even up to a few percents. Also, the shapes of MPPT curves depend on the sample. Fig. 8b illustrates the MPPT results for a longer time (approximately one day, measured in line with the ISOS–L–1 protocol [25]) drawn for the best two samples with Br and Cl. The Cs–Br solar cell exhibits a continuous increase of MPP during few first hours and this parameter saturates around approximately 16%. This tendency can be explained by the light soaking effect which decreases the bulk recombination defect density during illumination [51, 52, 53]. The MPPT curve for FA–Cl sample subtly decreases for the first two hours. However, further it starts to increase and reaches the maximum value (around 15.5%) after approximately 8 hours. Later, it keeps a constant magnitude for the next few hours and finally drops below 14%. This behavior can be related to the needles shape structures visible on the perovskite surface in the SEM image (Fig. 2). However, the last range of the MPP decreasing might originate from a diffusion of ions in the perovskite layer. It has been demonstrated that a migration of ionic species leads to the drop of the MPPT [54, 55, 56, 57, 58]. In general, the influence of both intrinsic and extrinsic ions should be taken into account. Here, we cannot exclude the Cu migration from the electrode into the perovskite.

## 4. Conclusions

The perovskite solar cells with two dual cation perovskites $Cs_{0.15}FA_{0.85}Pb(I_{0.95}Cl_{0.05})_3$ and $Cs_{0.15}FA_{0.85}Pb(I_{0.95}Br_{0.05})_3$ were investigated. The different sources of bromine atoms (CsBr, $PbBr_2$, FABr) and chlorine atoms (CsCl, $PbCl_2$, FACl) have been used for preparation of perovskite layers. All PSCs were fabricated using a two–step sequential deposition method. The photoelectrical results obtained for bromide–based devices lead to similar conclusions as for samples synthesized using one–step process [22]. However, the source of halogens has a less pronounced effect on PCE for the two–step technique. This is explained by a nucleation site in the inorganic layer that improves the growth of a perovskite. The chloride photocells are worse by the meaning of performance and time stability in comparison to bromide–based devices. The reason of this effect can be associated with the chlorines accumulation at the interface between the perovskite and PCBM. As a consequence, it leads to a higher interface recombination and a band–bending process. In addition, the bulk defect density is higher for all chloride samples if compared to the bromide ones. The results obtained in this work can be useful for further studies toward most efficient and stable perovskite solar cells.

## 5. Acknowledgement

This work has been supported by Solliance, a partnership of R&D organizations from the Netherlands, Belgium, and Germany working in thin film photovoltaic solar energy. The part of research has been also financed by a grant (2018/29/N/ST7/02326) sponsored by National Science Centre, Poland. Financial support was also provided by the Ministry of Science and Technology of Taiwan (MOST) with the project number 110-2222-E-002-001-MY3. In addition, the Early Research Program 'Sustainability & Reliability for solar and other (opto–)electronic thin–film devices' (STAR) from TNO is also acknowledged for funds. The authors would like to thank Igor Żukowicz for his help with the graphic design of TOC/abstract graphics.

## 6. Supplementary data

Supplementary data to this article can be found online at...

## References


[1] X. Zhu, D. Yang, R. Yang, B. Yang, Z. Yang, X. Ren, J. Zhang, J. Niu, J. Feng, S.(F.) Liu, Superior stability for perovskite solar cells with 20% efficiency using vacuum co–evaporation, Nanoscale 9 (2017) 12316–12323.

[2] F. Zhang, Z. Wang, H. Zhu, N. Pellet, J. Luo, C. Yi, X. Liu, H. Liu, S. Wang, X. Li, Y. Xiao, S.M. Zakeeruddin, D. Bi, M. Grätzel, Over 20% PCE perovskite solar cells with superior stability achieved by novel and low–cost hole–transporting materials, Nano Energy 41 (2017) 469–475.

[3] S.S. Shin, E.J. Yeom, W.S. Yang, S. Hur, M.G. Kim, J. Im, J. Seo, J.H. Noh, S.I. Seok, Colloidally prepared La–doped $BaSnO_3$ electrodes for efficient, photostable perovskite solar cells, Science 356 (2017) 167–171.

[4] M. Saliba, J.–P. Correa–Baena, C.M. Wolff, M. Stolterfoht, N. Phung, S. Albrecht, D. Neher, A. Abate, How to make over 20% efficient perovskite solar cells in regular (n–i–p) and inverted (p–i–n) architectures, Chem. Matter. 30 (2018) 4193–4201.

[5] T. Matsui, T. Yamamoto, T. Nishihara, R. Morisawa, T. Yokoyama, T. Sekiguchi, T. Negami, Compositional engineering for thermally stable, highly efficient perovskite solar cells exceeding 20% power conversion efficiency with 85 ∘C/85% 1000 h stability, Adv. Matter. 31 (2019) 1806823.

[6] Y. Li, R.L.Z. Hoye, H.–H. Gao, L. Yan, X. Zhang, Y. Zhou, J.L. MacManus–Driscoll, J. Gan, Over 20% efficiency in methylammonium lead iodide perovskite solar cells with enhanced stability via 'in situ solidification' of the $TiO_2$ compact layer, ACS Appl. Mater. Interfaces 12 (2020) 12 7135–7143.

[7] Y. Vaynzof, The future of perovskite photovoltaics – thermal evaporation or solution processing ?, Adv. Energy Mater. 10 (2020) 2003073.

[8] J. Burschka, N. Pellet, S.–J. Moon, R. Humphry–Baker, P. Gao, M. Nazeeruddin, M. Grätzel, Sequential deposition as a route to high–performance perovskite–sensitized solar cells, Nature 499 (2013) 316–320.

[9] J.–H. Im, H.–S. Kim, N.–G. Park, Morphology–photovoltaic property correlation in perovskite solar cells: One–step versus two–step deposition of $CH_3NH_3PbI_3$, APL Mater. 2 (2014) 80811510.

[10] J.–H. Im, I.–H. Jang, N. Pellet, M. Grätzel, N.–G. Park, Growth of $CH_3NH_3PbI_3$ cuboids with controlled size for high–efficiency perovskite solar cells, Nature Nanotechnology 9 (2014) 927–932.

[11] W.S. Yang, J.H. Noh, N.J. Jeon, Y. C. Kim, S. Ryu, J. Seo, S.I. Seok, High–performance photovoltaic perovskite layers fabricated through intramolecular exchange, Science 348 (2015) 1234–1237.

[12] Z. Yang, B. Cai, B. Zhou, T. Yao, W. Yu, S. Liu, W.–H. Zhang, C. Li, An up–scalable approach to $CH_3NH_3PbI_3$ compact films for high–performance perovskite solar cells, Nano Energy 15 (2015) 670–678.

[13] N. Yantara, D. Sabba, F. Yanan, J.M. Kadro, T. Moehl, P.P. Boix, S. Mhaisalkar, M. Grätzel, C. Grätzel, Loading of mesoporous titania films by $CH_3NH_3PbI_3$ perovskite, single step vs. sequential deposition, Chem. Commun. 51 (2015) 4603–4606.

[14] Q. Jiang, L. Zhang, H. Wang, X. Yang, J. Meng, H. Liu, Z. Yin, J. Wu, X. Zhang, J. You, Enhanced electron extraction using $SnO_2$ for high–efficiency planar–structure $HC(NH_2)_2PbI_3$–based perovskite solar cells, Nature Energy 2 (2016) 16177.

[15] M.R. Ahmadian–Yazdi, F. Zabihi, M. Habibi, M. Eslamian, Effects of process parameters on the characteristics of mixed–halide perovskite solar cells

fabricated by one–step and two–step sequential coating, Nanoscale Res. Lett. 11 (2016) 408.

[16] W. S. Yang, B.–W. Park, E.H. Jung, N.J. Jeon, Y.C. Kim, D.U. Lee, S.S. Shin, J. Seo, E.K. Kim, J.H. Noh, S.I. Seok, Iodide menagement in formamidinium–lead–halide–based perovskite layers for efficient solar cells, Science 356 (2017) 1376–1379.

[17] X. Zheng, B. Chen, J. Dai, Y. Fang, Y. Bai, Y. Lin, H. Wei, X.C. Zeng, J. Huang, Defect passivation in hybrid perovskite solar cells using quaternary ammonium halide anions and cations, Nature Energy 2 (2017) 17102.

[18] M. Li, Y.–M. Xie, X. Xu, Y. Huo, S.–W. Tsang, Q.–D. Yang, Y. Cheng, Comparison of processing windows and electronic properties between $CH_3NH_3PbI_3$ perovskite fabricated by one–step and two–step solution process, Org. Electron. 63 (2018) 159–165.

[19] Q. Li, Y. Zhao, R. Fu, W. Zhou, Y. Zhao, X. Liu, D. Yu, Q. Zhao, Efficient perovskite solar cells fabricated through CsCl–enhanced $PbI_2$ precursor via sequential deposition, Adv. Mater. 30 (2018) 1803095.

[20] A. Ummadisingu, M. Grätzel, Revealing the detailed path of sequential deposition for metal halide perovskite formation, Science Adv. 4 (2018) e1701402.

[21] L. Zheng, Y. Ma, S. Chu, S. Wang, B. Qu, L. Xiao, Z. Chen, Q. Gong, Z. Wu, X. Hou, Improved light absorption and charge transport for perovskite solar cells with rough interfaces by sequential deposition, Nanoscale 6 (2014) 8171–8176.

[22] D. Głowienka, F. Di Giacomo, M. Najafi, I. Dogan, A. Mameli, F.J.M. Colberts, J. Szmytkowski, Y. Galagan, Effect of different bromine sources on the dual cation mixed halides perovskite solar cells, ACS Appl. Energy Mater. 3 (2020) 8285–8294.

[23] D. Koushik, W.J.H. Verhees, Y. Kuang, S. Veenstra, D. Zhang, M.A. Verheijen, M. Creatore, R.E.I. Schropp, High–efficiency humidity–stable planar perovskite solar cells based on atomic layer architecture, Energy Environ. Sci. 10 (2017) 91–100.

[24] D. Głowienka, D. Zhang, M. Najafi, F. Di Giacomo, J. Szmytkowski, Y. Galagan, Impact of the trap–assisted recombination in the perovskite solar cells, in: 47th IEEE Photovoltaic Specialists Conference (PVSC 47), 2020, pp. 0629–0632.

[25] M.V. Khenkin, E.A. Katz, A. Abate, G. Bardizza, J.J. Berry, C. Brabec, F. Brunetti, V. Bulović, Q. Burlingame, A. Di Carlo, R. Cheacharoen, Y.–B. Cheng, A. Colsmann, S. Cros, K. Domanski, M. Dusza, C.J. Fell, S.R. Forrest, Y. Galagan, D. Di Girolamo, M. Grätzel, A. Hagfeldt, E. von Hauff, H. Hoppe, J. Kettle, H. Köbler, M.S. Leite, S. (F.) Liu, Y.–L. Loo, J.M. Luther, C.–Q. Ma, M. Madsen, M. Manceau, M. Matheron, M. McGehee, R. Meitzner, M.K. Nazeeruddin, A.F. Nogueira, Ç. Odabaşi, A. Osherov, N.–G. Park, M.O. Reese, F. De Rossi, M. Saliba, U.S. Schubert, H.J. Snaith, S.D. Stranks, W. Tress, P.A. Troshin, V. Turkovic, S. Veenstra, I. Visoly–Fisher, A. Walsh, T. Watson, H. Xie, R. Yildirim, S.M. Zakeeruddin, K. Zhu, M. Lira–Cantu, Consensus statement for stability assessment and reporting for perovskite photovoltaics based on ISOS procedures, Nature Energy 5 (2020) 35–49.

[26] L. Gil–Escrig, C. Momblona, M.–G. La–Placa, P.P. Boix, M. Sessolo, H.J. Bolink, Vacuum deposited triple–cation mixed–halide perovskite solar cells, Adv. Energy Mater 8 (2018) 1703506.

[27] C.C. Stoumpos, C.D. Malliakas, M.G. Kanatzidis, Semiconducting tin and lead iodide perovskites: Phase transitions, high mobilities, and near–infrared photoluminescent properties, Inorg. Chem. 52 (2013) 9019–9038.

[28] M.P.U. Haris, S. Kazim, S. Ahmad, Low–temperature–processed perovskite

solar cells fabricated from presynthesized $CsFAPbI_3$ powder, ACS Appl. Energy Matter. 4 (2021) 2600–2606.

[29] M. Zhang, J.S. Yun, Q. Ma, J. Zheng, C.F.J. Lau, X. Deng, J. Kim, D. Kim, J. Seidel, M.A. Green, S. Huang, A.W.Y Ho–Baillie, High–efficiency rubidium–incorporated perovskite solar cells by gas quenching, ACS Energy Lett. 2 (2017) 438–444.

[30] M. Martynow, D. Głowienka, J. Szmytkowski, Y. Galagan, J. Guthmuller, Influence of orientational disorder on the optical absorption properties of the hybrid metal–halide perovskite $CH_3NH_3PbI_3$, ChemPhysChem 20 (2019) 3228–3237.

[31] D. Głowienka, D. Zhang, F. Di Giacomo, M. Najafi, S. Veenstra, J. Szmytkowski, Y. Galagan, Role of surface recombination in perovskite solar cells at the interface of HTL/$CH_3NH_3PbI_3$, Nano Energy 67 (2020) 104186.

[32] K.O. Kosmatos, L. Theofylaktos, E. Giannakaki, D. Deligiannis, M. Konstantakou, T. Stergiopoulos, Methylammonium chloride: A key additive for highly efficient, stable, and up–scalable perovskite solar cells, Energy Environ. Mater. 2 (2019) 79–92.

[33] H. Yu, F. Wang, F. Xie, W. Li, J. Chen, N. Zhao, The role of chlorine in the formation of $CH_3NH_3PBI_{3-x}Cl_x$ perovskite, Adv. Funct. Mater. 24 (2014) 7102–7108.

[34] Y. Wu, X. Li, S. Fu, L. Wan, J. Fang, Efficient methylammonium lead trihalide perovskite solar cells with chloroformamidinium chloride (Cl–FACl) as an additive, J. Mater. Chem. A 7 (2019) 8078–8084.

[35] Z. Li, C. Kolodziej, C. McCleese, L. Wang, A. Kovalsky, A.C. Samia, Y. Zhao, C. Burda, Effect of chloride substitution on interfacial charge transfer processes in $MAPbI_3$ perovskite thin film solar cells: Planar versus mesoporous, Nanoscale Adv. 1 (2019) 827–833.

[36] A. Suzuki, M. Kato, N. Ueoka, T. Oku, Additive effect of formamidinium chloride in methylammonium lead halide compound–based perovskite solar cells, J. Electron. Mater. 48 (2019) 3900–3907.

[37] L. Fan, Y. Ding, J. Luo, B. Shi, X. Yao, C. Wei, D. Zhang, G. Wang, Y. Sheng, Y. Chen, A. Hagfeldt, Y. Zhao, X. Zhang, Elucidating the role of chlorine in perovskite solar cells, J. Mater. Chem. A 5 (2017) 7423–7432.

[38] B. Yang, J. Keum, O.S. Ovchinnikova, A. Belianinov, S. Chen, M.–H. Du, I.N. Ivanov, C.M. Rouleau, D.B. Geohegan, K. Xiao, Deciphering halogen competition in organometallic halide perovskite growth, J. Am. Chem. Soc. 138 (2016) 5028–5035.

[39] S. Colella, E. Mosconi, P. Fedeli, A. Listorti, F. Gazza, F. Orlandi, P. Ferro, T. Besagni, A. Rizzo, G. Calestani, G. Gigli, F. De Angelis, R. Mosca, $MAPbI_{3-x}Cl_x$ mixed halide perovskite for hybrid solar cells: The role of chloride as dopant on the transport and structural properties, Chem. Mater. 25 (2013) 4613–4618.

[40] M.I. Dar, N. Arora, P. Gao, S. Ahmad, M. Grätzel, M.K. Nazeeruddin, Investigation regarding the role of chloride in organic–inorganic halide perovskites obtained from chloride containing precursors, Nano Lett. 14 (2014) 6991–6996.

[41] J. Byeon, J. Kim, J.–Y. Kim, G. Lee, K. Bang, N. Ahn, M. Choi, Charge transport layer–dependent electronic band bending in perovskite solar cells and its correlation to light–induced device degradation, ACS Energy Lett. 5 (2020) 2580–2589.

[42] J. Ding, J. Duan, C. Guo, Q Tang, Toward charge extraction in all–inorganic perovskite solar cells by interfacial engineering, J. Mater. Chem. A 6 (2018) 21999–22004.

[43] H. Kanda, N. Shibayama, A.J. Huckaba, Y. Lee, S. Paek, N. Klipfel, C. Roldan–Carmona, V.I.E. Queloz, G. Grancini, Y. Zhang, M. Abuhelaiqa,

K.T. Cho, M. Li, M.D. Mensi, S. Kinge, M.K. Nazeeruddin, Band–bending induced passivation: High performance and stable perovskite solar cells using a perhydropoly(silazane) precursor, Energy Environ. Sci. 13 (2020) 1222–1230.

[44] R. Saive, S–shaped current–voltage characteristics in solar cells: A review, IEEE Journal of Photovoltaics 9 (2019) 1477–1484.

[45] M. Mews, M. Liebhaber, B. Rech, L. Korte, Valence band alignment and hole transport in amorphous/crystalline silicone heterojunction solar cells, Appl. Phys. Lett. 107 (2015) 013902.

[46] A. Nakane, H. Tampo, M. Tamakoshi, S. Fujimoto, K.M. Kim, S. Kim, H. Shibata, S. Niki, H. Fujiwara, Quantitative determination of optical and recombination losses in thin–film photovoltaic devices based on external quantum efficiency analysis, J. Appl. Phys. 120 (2016) 064505.

[47] W. Tress, M. Yavari, K. Domanski, P. Yadav, B. Niesen, J.P.C. Baena, A. Hagfeldt, M. Grätzel, Interpretation and evolution of open–circuit voltage, recombination, ideality factor and subgap defect states during reversible light–soaking and irreversible degradation of perovskite solar cells, Energy Environ. Sci. 11 (2018) 151–165.

[48] P. Caprioglio, C.M. Wolff, O.J. Sandberg, A. Armin, B. Rech, S. Albrecht, D. Neher, M. Stolterfoht, On the origin of the ideality factor in perovskite solar cells, Adv. Energy Mater. 10 (2020) 20000502.

[49] N.E. Courtier, Interpreting ideality factors for planar perovskite solar cells: ectypal diode theory for steady–state operation, Phys. Rev. Appl. 14 (2020) 024031.

[50] W. Shockley, H.J. Queisser, Detailed balance limit of efficiency of p–n junction solar cells, J. Appl. Phys. 32 (1961) 510–519.

[51] H. Jin, E. Debroye, M. Keshavarz, I.G. Scheblykin, M.B.J. Roeffaers, J. Hofkens, J.A. Steele, It's a trap ! On the nature of localised states and charge trapping in lead halide perovskites, Mater. Horiz. 7 (2020) 397–410.

[52] X. Deng, X. Wen, J. Zheng, T. Young, C.F.J. Lau, J. Kim, M. Green, S. Huang, A. Ho–Baillie, Dynamic study of the light soaking effect on perovskite solar cells by in–situ photoluminescence microscopy, Nano Energy 46 (2018) 356–364.

[53] Y. Zhong, C.A.M. Luna, R. Hildner, C. Li, S. Huettner, In situ investigation of light soaking in organolead halide perovskite films, APL Mater. 7 (2019) 041114.

[54] K. Domanski, J.–P. Correa–Baena, N. Mine, M.K. Nazeeruddin, A. Abate, M. Saliba, W. Tress, A. Hagfeldt, M. Grätzel, Not all that glitters is gold: metal–migration–induced degradation in perovskite solar cells, ACS Nano 10 (2016) 6306–6314.

[55] Z. Li, C. Xiao, Y. Yang, S.P. Harvey, D.H. Kim, J.A. Christians, M. Yang, P. Schulz, S.U. Nanayakkara, C.–S. Jiang, J.M. Luther, J.J. Berry, M.C. Beard, M.M. Al–Jassima, K. Zhu, Extrinsic ion migration in perovskite solar cells, Energy Environ. Sci. 10 (2017) 1234–1242.

[56] X. Li, S. Ke, X.X Feng, X. Zhao, W. Zhang, J. Fang, Enhancing the stability of perovskite solar cells through cross–linkable and hydrogen bonding multifunctional additives, J. Mater. Chem. A 9 (2021) 12684–12689.

[57] W. Chen, B. Han, Q. Huc, M. Gu, Y. Zhu, W. Yang, Y. Zhou, D. Luo, F.–Z. Liu, R. Cheng, R. Zhu, S.–P. Feng, A.B. Djurišić, T.P. Russell, Z. He, Interfacial stabilization for inverted perovskite solar cells with long–term stability, Science Bulletin 66 (2021) 991-1002.

[58] Q. Cao, Y. Li, H. Zhang, J. Yang, J. Han, T. Xu, S. Wang, Z. Wang, B. Gao, J. Zhao, X. Li, X. Ma, S.M. Zakeeruddin, W.E.I. Sha, X. Li, M. Grätzel, Efficient and stable inverted perovskite solar cells with very high

Table 1: The materials used for synthesis of perovskites. The compounds needed to prepare all first layers were dissolved in 1 ml of DMF:DMSO with the ratio 9:1. The compounds to compose all second layers were dissolved in 1 ml of IPA.

| Perovskite | Layer | Compounds |
|---|---|---|
| Cs–Br | first: | 622.4 mg of $PbI_2$ + 43.1 mg of CsBr |
| | second: | 77.4 mg of FAI |
| Pb–Br | first: | 575.7 mg of $PbI_2$ + 37.2 mg of $PbBr_2$ + 52.6 mg of CsI |
| | second: | 77.4 mg of FAI |
| FA–Br | first: | 622.4 mg of $PbI_2$ + 52.6 mg of CsI |
| | second: | 65.8 mg of FAI + 8.4 mg of FABr |
| Cs–Cl | first: | 622.4 mg of $PbI_2$ + 34.1 mg of CsCl |
| | second: | 77.4 mg of FAI |
| Pb–Cl | first: | 575.7 mg of $PbI_2$ + 28.2 mg of $PbCl_2$ + 52.6 mg of CsI |
| | second: | 77.4 mg of FAI |
| FA–Cl | first: | 622.4 mg of $PbI_2$ + 52.6 mg of CsI |
| | second: | 65.8 mg of FAI + 5.4 mg of FACl |

fill factors via incorporation of star–shaped polymer, Sci. Adv. 7 (2021) eabg0633.

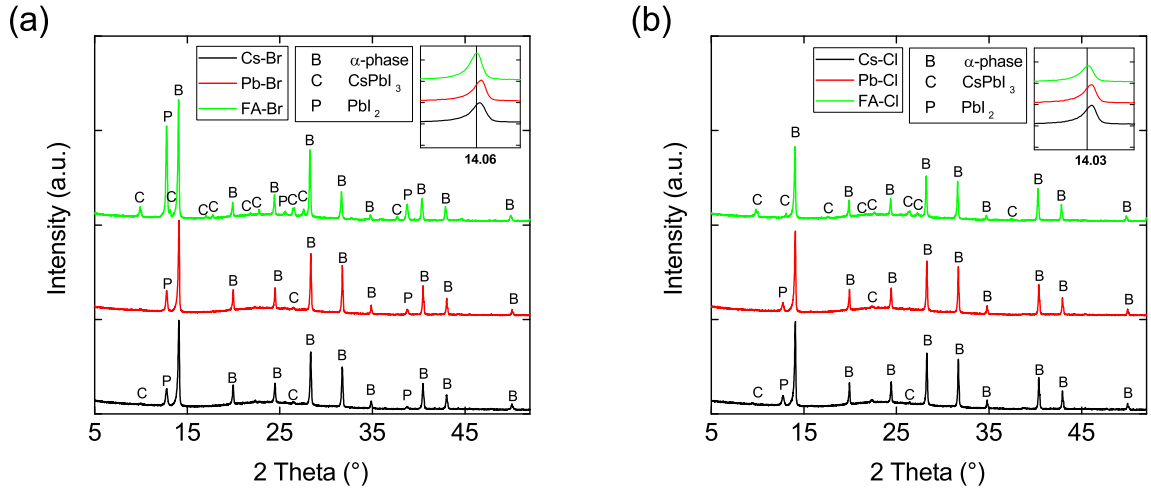


Figure 1: XRD patterns of the perovskite films on the glass substrate. (a) Results for $Cs_{0.15}FA_{0.85}Pb(I_{0.95}Br_{0.05})_3$ obtained from different bromides. (b) Results for $Cs_{0.15}FA_{0.85}Pb(I_{0.95}Cl_{0.05})_3$ obtained from different chlorides. Both insets show illustration of Vegard's law.

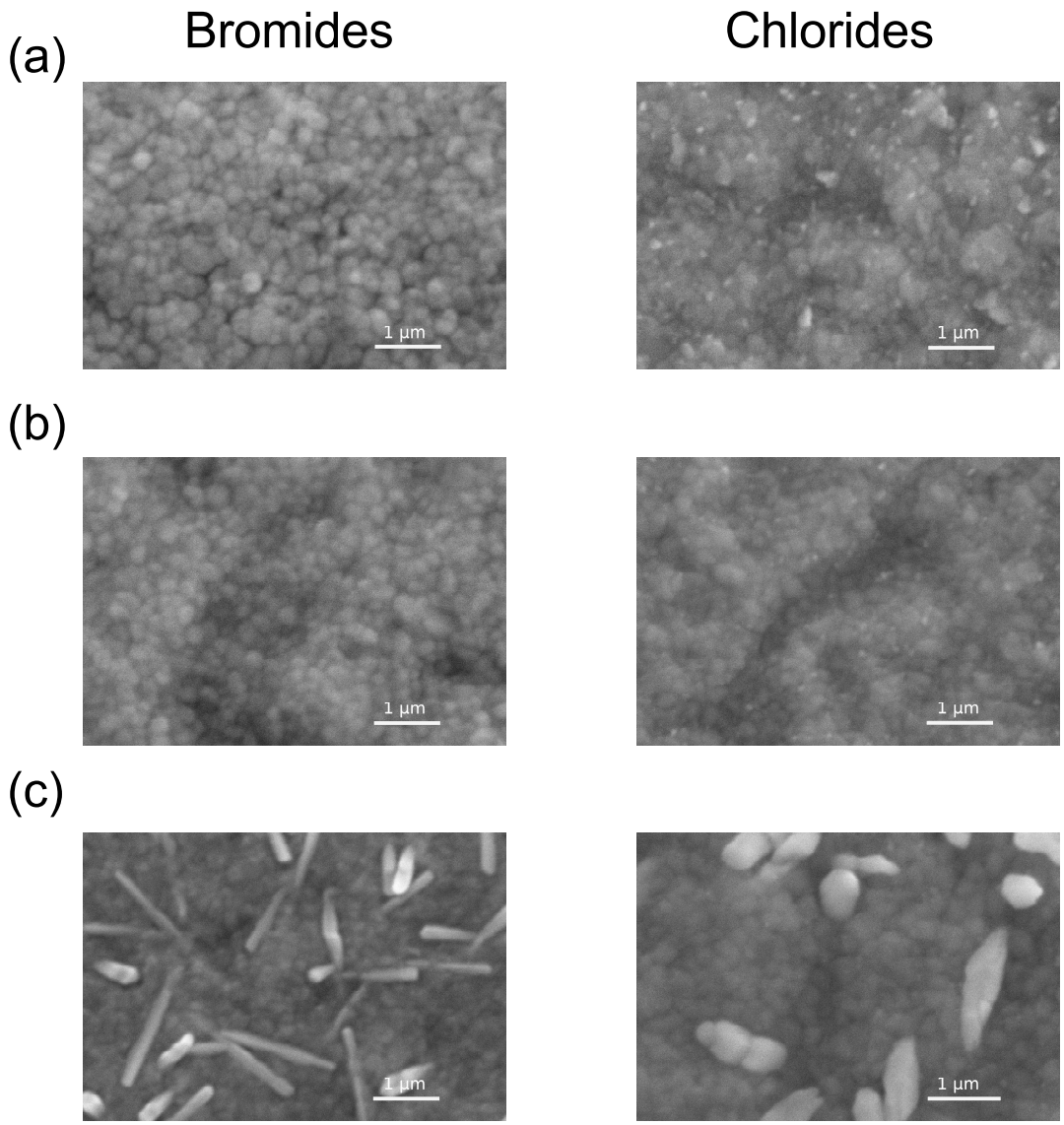


Figure 2: SEM images of all perovskite films prepared with (a) caesium–based compounds, (b) lead–based compounds, and (c) formamidinium–based compounds.

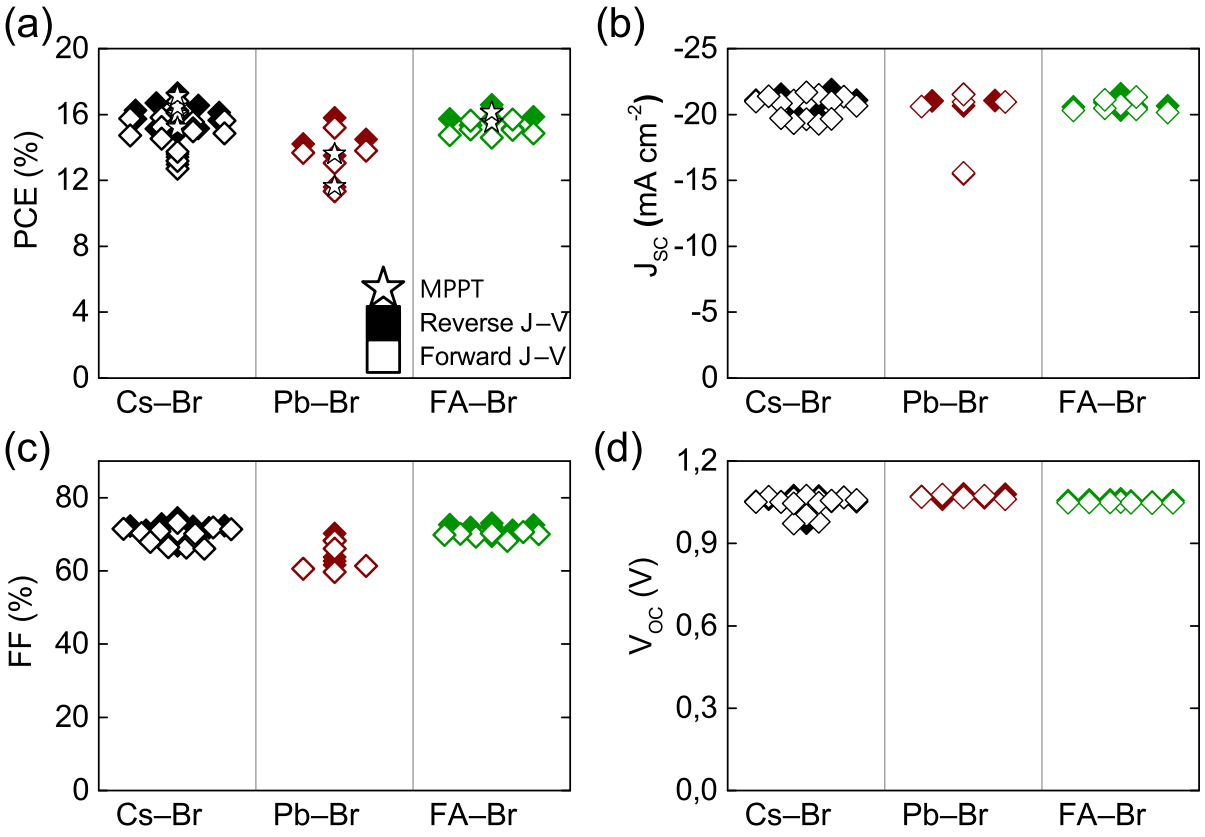


Figure 3: Four photovoltaic parameters of PSCs obtained with different sources of bromine atoms, (a) PCE, (b) $J_{sc}$, (c) FF, (d) $V_{oc}$.

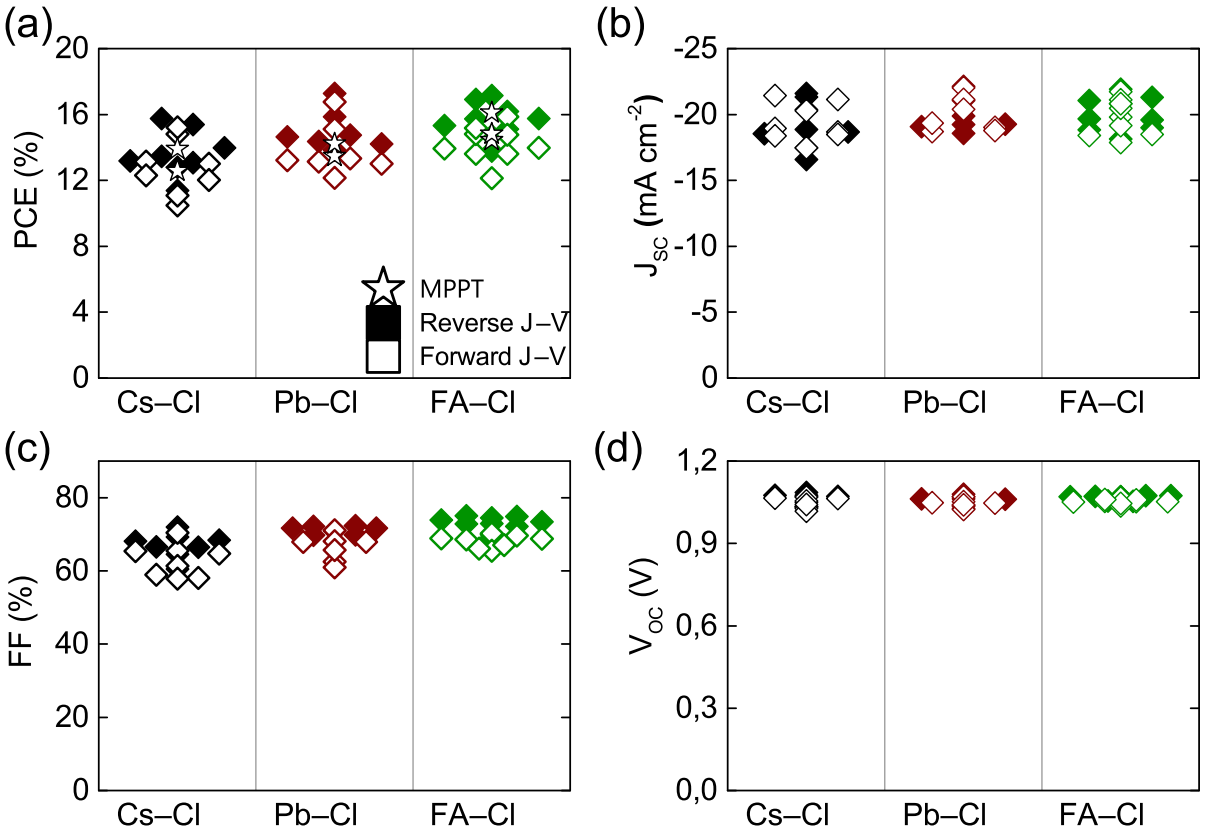


Figure 4: Four photovoltaic parameters of PSCs obtained with different sources of chlorine atoms, (a) PCE, (b) $J_{sc}$, (c) FF, (d) $V_{oc}$.

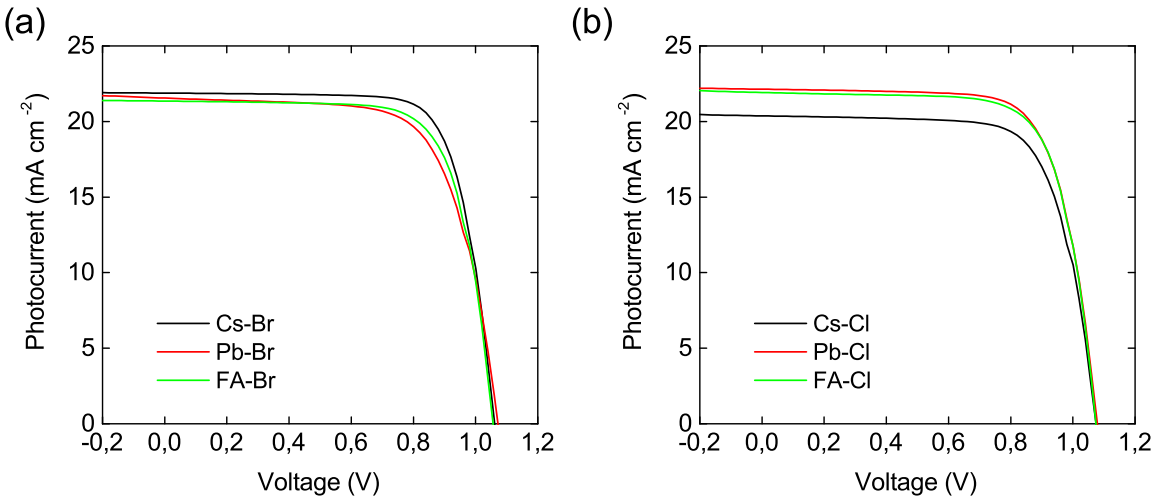


Figure 5: J–V characteristics for representative solar cell devices. (a) Results for $Cs_{0.15}FA_{0.85}Pb(I_{0.95}Br_{0.05})_3$ obtained from different bromides. (b) Results for $Cs_{0.15}FA_{0.85}Pb(I_{0.95}Cl_{0.05})_3$ obtained from different chlorides.

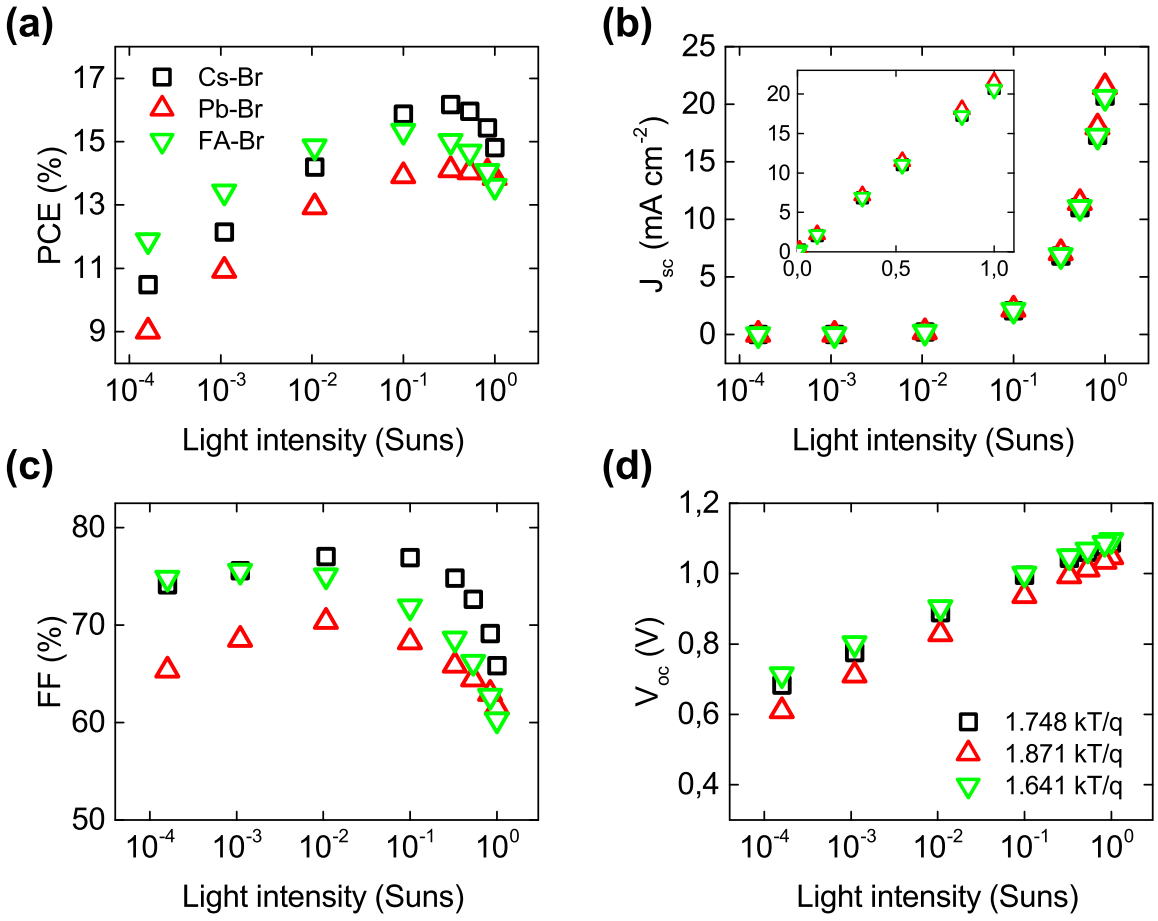


Figure 6: Four photovoltaic parameters versus light intensity drawn for representative solar cell devices obtained with different sources of bromine atoms, (a) PCE, (b) $J_{sc}$, (c) FF, (d) $V_{oc}$. The ideality factors for all samples are written in part (d).

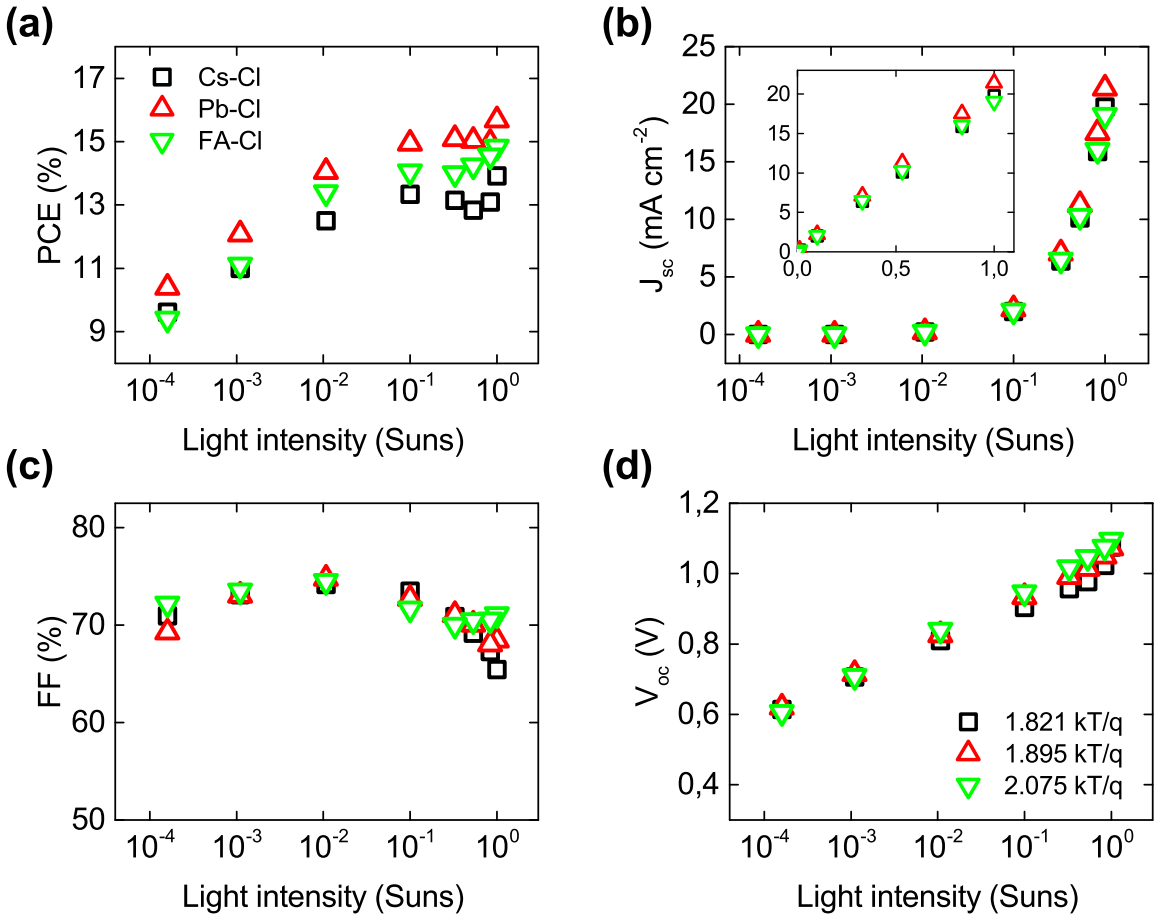


Figure 7: Four photovoltaic parameters versus light intensity drawn for representative solar cell devices obtained with different sources of chlorine atoms, (a) PCE, (b) $J_{sc}$, (c) FF, (d) $V_{oc}$. The ideality factors for all samples are written in part (d).

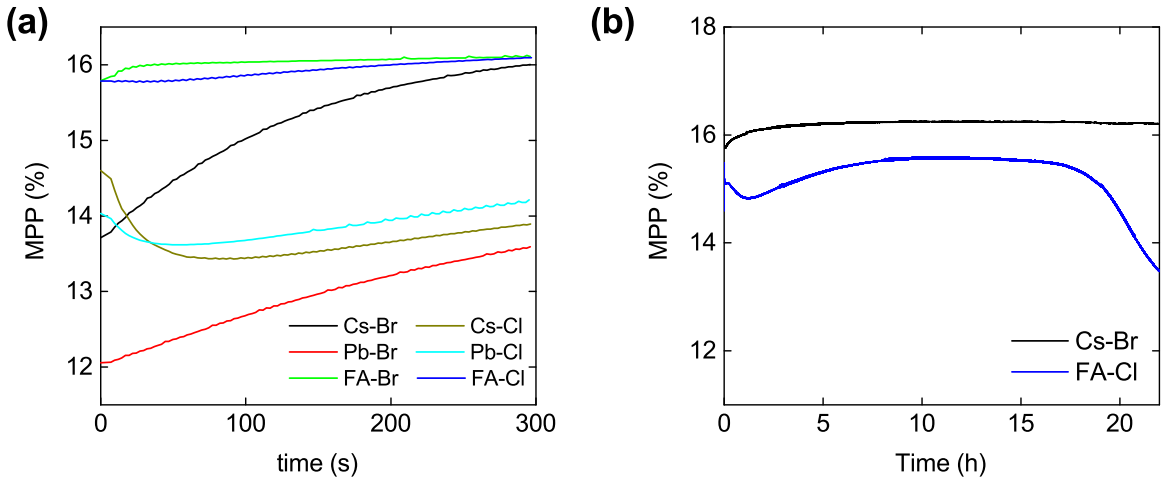


Figure 8: Maximum Power Point Tracking (MPPT) measurements of best performing solar cells. (a) Results for a short period obtained for all PSCs. (b) Results for a longer period obtained for two representative samples with bromine and chlorine atoms.